

Effective Photodissociation Cross Sections for Molecular Oxygen and Nitric Oxide in the Schumann-Runge Bands

MARK ALLEN

Division of Geological and Planetary Sciences, California Institute of Technology, Pasadena, CA 91125

JOHN E. FREDERICK

Laboratory for Planetary Atmospheres, NASA/Goddard Space Flight Center, Greenbelt, MD 20771

(Manuscript received 22 September 1981, in final form 7 June 1982)

ABSTRACT

Simple polynomial representations of the altitude and zenith angle dependence of effective photodissociation cross sections for molecular oxygen and nitric oxide in the Schumann-Runge band region are presented. Longward of ~ 202 nm, the atmosphere is optically thin and the effective cross sections are well correlated with local temperature. Atmospheric transmission values and O_2 and NO photodissociation rates calculated using the parameterized effective cross sections are in good agreement with the results of the high spectral resolution computations of Frederick and Hudson. The effective cross section approach allows the use of different solar spectra and avoids the assumption of previous work that ray paths at different solar zenith angles, but with the same O_2 absorbing column, have the same opacity and dissociation rates. The errors resulting from this assumption can exceed 20% at optical depths greater than 2.

1. Introduction

Accurate calculations of the atmospheric opacity and the photodissociation rate of molecular oxygen in the Schumann-Runge bands (175–205 nm) are necessary for modeling chemistry in the terrestrial upper atmosphere. Details of the attenuation of solar flux in this spectral range affect the dissociation of certain trace species, for example, nitric oxide and water. In this paper, we will present simple formulations appropriate for photochemical models of the middle atmosphere.

The rotational structure of the Schumann-Runge bands requires that calculations of transmission and O_2 photodissociation have high spectral resolution. A number of recent studies (Kockarts, 1976; Blake, 1979; Nicolet and Peetermans, 1980; Frederick and Hudson, 1980a,b) have reported the results of such detailed computations, which have increased accuracy compared to previous work. There are two problems which generally make these published results difficult to utilize. First, the volume of data that needs to be stored to reproduce a variety of solar zenith angles is very large. Second, the O_2 photodissociation rates tabulated incorporate the author's choice of solar flux at the top of the atmosphere and therefore cannot easily be adapted for computations at different solar conditions.

A more useful approach for modeling is to develop parameterizations based on the results of detailed

computations which can then be used directly to calculate transmission and O_2 dissociation rates for different conditions. Although average cross sections are useful for understanding the molecular physics (Kockarts, 1971), effective cross sections, which reflect optical depth effects and therefore vary with absorbing O_2 column, are needed for the aeronomy calculations (Hudson *et al.*, 1969; Anderson, 1971; Kockarts, 1971). Park (1974) found that two sets of cross sections are required to reproduce both the transmission and O_2 photodissociation variation with altitude. Both Kockarts (1976) and Blake (1979) also present two sets of results in order to calculate both transmission and O_2 photodissociation. According to Logan *et al.* (1978), one set of effective cross sections can be used in both calculations, but unfortunately the opacity functions they employ are not consistent with more recent work.

In all of this previous work, the assumption has been made that the transmission and O_2 dissociation rates are a function only of absorbing O_2 column. This is true for an isothermal atmosphere. But because the detailed O_2 Schumann-Runge band cross sections are temperature-dependent and the atmosphere is not isothermal, optical paths with the same column of O_2 , but different zenith angles, may have significantly different transmission and dissociation rates. Detailed calculations at different zenith angles done for this work show that values for ray paths with different zenith angles but the same O_2 column

TABLE 1. Spectral region of O₂ Schumann-Runge bands.

Interval I_i	Range of I_i	
	(cm ⁻¹)	(nm)
1	48 600-49 000	204.1-205.8
2	49 000-49 500	202.0-204.1
3	49 500-50 000	200.0-202.0
4	50 000-50 500	198.0-200.0
5	50 500-51 000	196.1-198.0
6	51 000-51 500	194.2-196.1
7	51 500-52 000	192.3-194.2
8	52 000-52 500	190.5-192.3
9	52 500-53 000	188.7-190.5
10	53 000-53 500	186.9-188.7
11	53 500-54 000	185.2-186.9
12	54 000-54 500	183.5-185.2
13	54 500-55 000	181.8-183.5
14	55 000-55 500	180.2-181.8
15	55 500-56 000	178.6-180.2
16	56 000-56 500	177.0-178.6
17	56 500-57 000	175.4-177.0

will differ by more than 20% for optical depths ≥ 2 , i.e., at mesospheric altitudes. In this paper, we present a single simple parameterization of effective cross sections that can be used to calculate both O₂ opacity and dissociation rates and we introduce a zenith angle dependent factor that accounts for variations shown in detailed calculations. Our analysis is based on the results of Frederick and Hudson (1980a,b) rather than Nicolet and Peetermans (1980) because the former work used more current values for the spectroscopic parameters of molecular oxygen. Furthermore, the cross sections of Frederick and Hudson (1980a,b) predict attenuated solar irradiances which are in satisfactory agreement with balloon measurements in the stratosphere (Frederick *et al.*, 1981).

A number of nitric oxide absorption bands fall in the spectral range of the O₂ Schumann-Runge bands. Nicolet and Cieslik (1980) calculated the contributions of these different bands to the NO photodissociation rate and found that the delta bands are the most significant for the terrestrial upper atmosphere. Since the nitric oxide delta predissociation bands have sharp structure, high-resolution calculations are necessary for accurate evaluation of the NO photodissociation rates. The results of such computations have been recently reported by Frederick and Hudson (1979a), Nicolet (1979) and Nicolet and Cieslik (1980). Similar to the situation with the reported O₂ dissociation rates, the NO dissociation rates presented in these papers inextricably include the authors' choice for solar flux. A flux-independent number is calculated by Park (1974) and average cross sections are given by Logan *et al.* (1978). These various approaches, however, do not reproduce the detailed zenith angle dependent calculations of Frederick and Hudson (1979a), so we present here simple parameterizations of NO effective cross sections and

zenith angle correction factors that agree with the detailed results.

2. Molecular oxygen effective cross sections

The Schumann-Runge bands dominate the 48 600–57 000 cm⁻¹ spectral region. Underlying these bands are the Schumann-Runge and Herzberg continua, which also need to be included in all calculations of atmospheric opacity and O₂ photodissociation rates. For simplicity, the spectral range of the Schumann-Runge bands can be subdivided into seventeen 400 or 500 cm⁻¹ intervals I_i (Table 1). For each interval, over the altitude range $z = 20$ –120 km, Frederick and Hudson (1980a) tabulate the atmospheric transmission $T_i(z)$ due to vertical O₂ opacity (solar zenith angle $\chi = 0^\circ$).¹ For the current work, additional calculations of $T_i(z)$ at $\chi = 30, 60$ and 85° were made. Molecular oxygen photodissociation rates $J_i(z)$ at $\chi = 0^\circ$ are tabulated in Frederick and Hudson (1980b) for $z = 20$ –60 km. For the current work, the solar flux at infinity was set to unity and $J_i(z)$ values independent of a particular choice of solar flux were calculated at $\chi = 0, 30, 60$ and 85° for $z = 20$ –120 km using the cross sections of Frederick and Hudson (1980b). Now an effective cross section σ_i^e can be defined which simultaneously satisfies the two relationships

$$T_i(z, \chi) = T_i(z + \Delta z, \chi) \exp\{-\frac{1}{2}[\sigma_i^e(z, \chi) + \sigma_i^e(z + \Delta z, \chi)][N(z) - N(z + \Delta z)] \sec \chi\}, \quad (1)$$

$$J_i(z, \chi) = \sigma_i^e(z, \chi) T_i(z, \chi) \Delta_i, \quad (2)$$

where $N(z)$ is the zenith O₂ column above altitude z and Δ_i is the wavelength extent of interval I_i . Since the value of the solar flux per Angstrom was set to unity in calculating J_i , Δ_i is in units of angstroms. The values of $\sigma_i^e(z, \chi)$ thus computed for the 17 spectral intervals are plotted in Fig. 1. For large zenith angles, the transmission becomes zero at low altitudes, so the effective cross sections could not be calculated. At the highest altitudes, the effective cross sections are the average cross sections for the interval. Indeed, the high-altitude values plotted in Fig. 1 are close to the mean cross sections of Kockarts (1976) for corresponding spectral intervals. At high optical depths (low altitude points), $\sigma_i^e(z, \chi)$ for different χ are practically the same and equal to the underlying continuum arising from the Schumann-Runge and Herzberg continua and the broad line wings of the Schumann-Runge band rotational lines. The values for $\sigma_i^e(20 \text{ km}, \chi)$ are close to the average continuum values of comparable spectral intervals in the O₂ absorption spectrum in Kockarts (1971).

As seen in Fig. 1, the variation of σ_i^e with altitude

¹ There are two typographical errors in Table A2 of Frederick and Hudson (1980a). $T_1(20 \text{ km})$ should be 4.902×10^{-2} and $T_6(20 \text{ km})$ should be 4.392×10^{-3} .

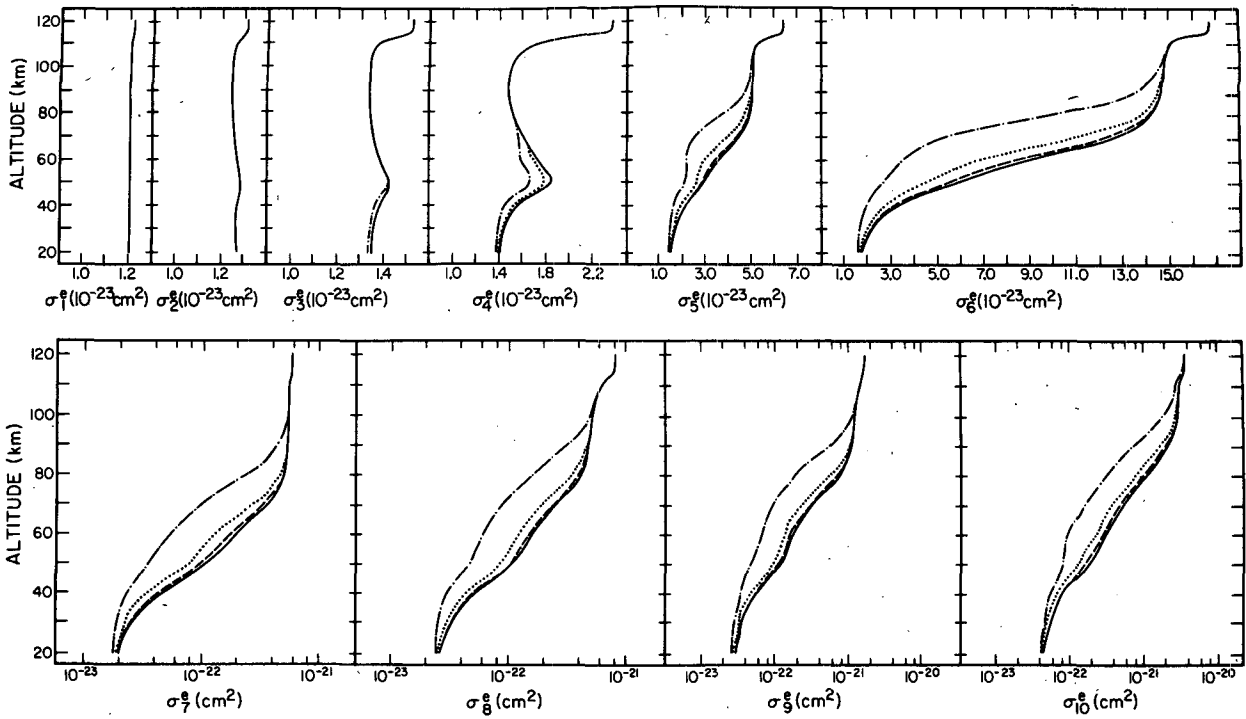


FIG. 1a. Molecular oxygen effective cross sections $\sigma_i^o(z, \chi)$, $i = 1-10$, calculated from the results of high spectral resolution computations, for solar zenith angle $\chi = 0^\circ$ (solid line), 30° (dashed), 60° (dotted) and 85° (dot-dashed).

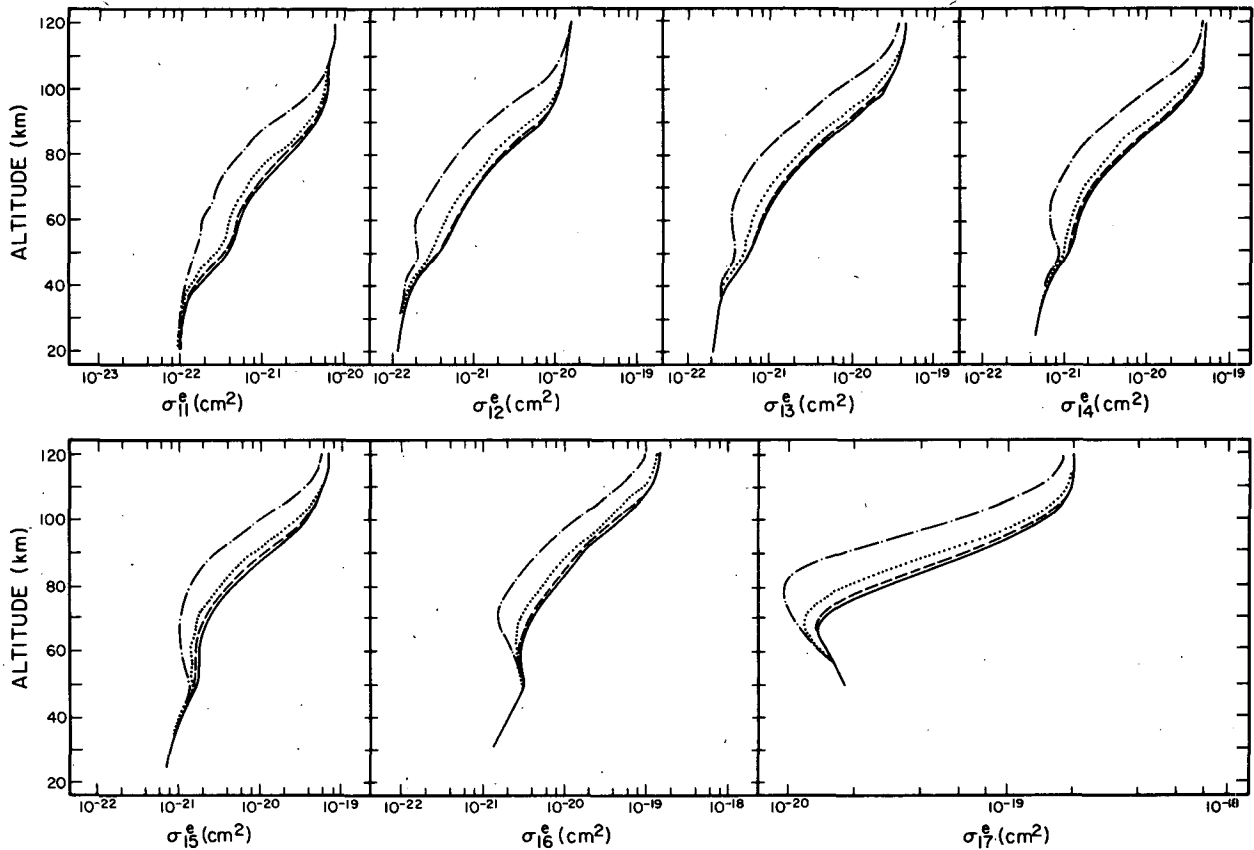


FIG. 1b. As in 1a, except for $i = 11-17$.

TABLE 2. Parametrization of O₂ effective photodissociation cross sections σ_i^e*

I _i	X _i [†]	Polynomial coefficients										Maximum error of fit
		a ₁₁	a ₁₂	a ₁₃	a ₁₄	a ₁₅	a ₁₆	a ₁₇	a ₁₈	a ₁₉	a ₂₀	
1	T(z)	-2.291902(+1)‡	1.177283(-4)	-2.191960(-4)	6.129866(-7)	-6.227325(-10)	4.169606(-3)	-7.126663(-3)	-2.263652(-3)	-1.971653(-4)	1% at 120 km	
2	T(z)	-2.292537(+1)	3.411511(-2)	-1.007612(-1)	2.404666(-2)	4.761876(-2)	4.169606(-3)	-7.126663(-3)	-2.263652(-3)	-1.971653(-4)	1% at 115 km	
3	T(z)	-2.483327(+1)	-5.823677(-2)	-1.094205(-2)	2.079595(-2)	3.769638(-3)	4.169606(-3)	-7.126663(-3)	-2.263652(-3)	-1.971653(-4)	1% at 20 km	
4	log ₁₀ P(z)	-2.275072(+1)	-2.054719(-1)	-1.094205(-2)	2.079595(-2)	3.769638(-3)	4.169606(-3)	-7.126663(-3)	-2.263652(-3)	-1.971653(-4)	8% at 115 km	
5	log ₁₀ P(z)	-2.256145(+1)	-3.960759(-1)	-2.995798(-2)	4.918104(-2)	9.269081(-3)	-1.173411(-3)	-2.599386(-4)	-3.069686(-4)	-3.069686(-4)	6% at 115 km	
6	log ₁₀ P(z)	-2.228000(+1)	-3.707936(-1)	-3.30207(-2)	5.959032(-2)	1.510540(-2)	1.000376(-3)	-2.599386(-4)	-3.069686(-4)	-3.069686(-4)	5% at 110 km	
7	log ₁₀ P(z)	-2.205261(+1)	-4.400848(-1)	-5.687308(-3)	3.712279(-2)	6.025527(-3)	1.179966(-2)	-8.296877(-3)	-3.238368(-3)	-3.069686(-4)	8% at 25 km	
8	log ₁₀ P(z)	-2.205327(+1)	-4.400848(-1)	-5.687308(-3)	3.712279(-2)	6.025527(-3)	1.179966(-2)	-8.296877(-3)	-3.238368(-3)	-3.069686(-4)	11% at 50 km	
9	log ₁₀ P(z)	-2.200507(+1)	-4.628729(-1)	-5.022541(-2)	2.545036(-2)	5.791406(-2)	1.179966(-2)	-8.296877(-3)	-3.238368(-3)	-3.069686(-4)	9% at 50 km	
10	log ₁₀ P(z)	-2.184813(+1)	-4.753880(-1)	4.519945(-2)	3.228313(-2)	3.079373(-3)	1.179966(-2)	-8.296877(-3)	-3.238368(-3)	-3.069686(-4)	14% at 55 km	
11	log ₁₀ P(z)	-2.158311(+1)	-4.164652(-1)	5.266362(-2)	1.655877(-2)	1.655877(-2)	1.179966(-2)	-8.296877(-3)	-3.238368(-3)	-3.069686(-4)	22% at 50 km	
12	log ₁₀ P(z)	-2.153128(+1)	-4.147369(-1)	7.763767(-2)	1.905438(-2)	1.905438(-2)	1.179966(-2)	-8.296877(-3)	-3.238368(-3)	-3.069686(-4)	16% at 50 km	
13	log ₁₀ P(z)	-2.129869(+1)	-4.063352(-1)	-2.178907(-2)	5.974212(-2)	5.974212(-2)	1.179966(-2)	-8.296877(-3)	-3.238368(-3)	-3.069686(-4)	8% at 50 km	
14	log ₁₀ P(z)	-2.101413(+1)	-3.395648(-1)	-4.150888(-2)	1.251500(-2)	4.081477(-2)	1.179966(-2)	-8.296877(-3)	-3.238368(-3)	-3.069686(-4)	9% at 40 km	
15	log ₁₀ P(z)	-2.081294(+1)	-1.974461(-1)	-1.463684(-1)	-3.650741(-2)	5.925899(-2)	2.323992(-2)	2.26029(-2)	2.26029(-2)	2.26029(-2)	11% at 50 km	
16	log ₁₀ P(z)	-2.052518(+1)	-8.193594(-2)	-2.809525(-1)	-2.825028(-1)	7.845485(-2)	1.59252(-1)	6.406164(-2)	1.107629(-2)	7.059213(-4)	7% at 50 km	
17	log ₁₀ P(z)	-1.973602(+1)	-8.092201(-2)	-4.839265(-1)	-1.041207(-1)	3.939418(-1)	2.984836(-1)	9.159857(-2)	1.333237(-2)	7.600642(-4)	1% at 100 km	

* log₁₀σ_i^e(z, χ = 0°) = ∑ a_{ij}X_i(z)^{j-1}

† Local atmosphere parameter at altitude z, either temperature T(z) or pressure P(z) in units of K or mb, respectively.

‡ Read -2.291902(+1) as -2.291902 × 10⁺¹.

depends on the particular interval I_i. The vertical variation in Fig. 1 is very similar to what was calculated by Anderson (1971). To investigate the altitude-dependence of σ_i^e, we sought correlations of σ_i^e(z, χ = 0°) with local atmospheric variables, temperature T(z) and pressure P(z). In the longest wavelength intervals, the opacity is small and the effective cross sections are close to the average values. In the case of I₁, σ₁^e is relatively constant over the whole altitude range. Kockarts (1976) shows that the mean cross sections for the longest wavelength intervals are the most sensitive to temperature. The temperature sensitivity arises because 1) absorption in the Schumann-Runge bands is due to transitions from the ν'' = 0 and ν'' = 1 levels of the X³Σ_g⁻ state of O₂ (Kockarts, 1971), a change in temperature will affect the relative populations of these vibrational states, and 2) temperature determines the relative populations of the rotational levels in each of the ν'' states and thus affects the band shape (Kockarts, 1976). A temperature correlation would then be expected in our data and is seen in the cases of σ₂₋₄^e. As a result, the variation of σ₂^e and σ₃^e can be parameterized well as a function of local temperature. Unfortunately, the relationship of σ₄^e with temperature is complicated. At the shorter wavelengths, i ≥ 4, opacity effects become large and σ_i^e therefore deviates from the average value in the stratosphere and mesosphere. The variation of σ_i^e with altitude could best be related to the pressure level (or equivalently, the absorbing O₂ column). The altitude variation of the zenith effective cross sections can be well fit by simple polynomial expressions of the type

$$\log_{10}\sigma_i^e(z, \chi = 0^\circ) = \sum_j a_{ij}X_i(z)^{j-1}, \quad (3)$$

where X_i(z) is either T(z) or log₁₀P(z) (from U.S. Standard Atmosphere, 1976) (units of K or mb, respectively). The coefficients a_{ij}, determined by a least-squares fit, are presented in Table 2.² The average errors of the least-squares fits are much smaller than the maximum errors reported in this table (for example, in the case of I₁₁, the error averaged over all altitudes is 9% whereas the maximum error is 22%) and are well within the uncertainties of the original detailed calculations (Frederick and Hudson, 1980a,b).

As discussed in the previous section, the O₂ opacity and dissociation does vary with zenith angle in a manner that cannot always be correlated with absorbing O₂ column (i.e., ray paths with the same O₂ column do not necessarily have the same values due to temperature variations along the path). We found that the σ_i^e(z, χ) variation with χ can be simply represented as

² Effective oxygen cross sections σ_i^ec cannot be calculated using the polynomial approximations (3) for altitudes at which σ_i^e is not plotted in Fig. 1.

TABLE 3. Parametrization of zenith-angle dependence of O₂ effective photodissociation cross sections.*

I_i	Polynomial coefficients					Maximum error of fit
	b_{1i}	b_{2i}	b_{3i}	b_{4i}	b_{5i}	
1	-2.996639					2% at 35 km, $\chi = 85^\circ$
2	-4.474937					1% at 35 km, $\chi = 85^\circ$
3	-2.535815					1% at 85 km, $\chi = 85^\circ$
4	3.033416(+3)†	-5.978911(+2)	4.370384(+1)	-1.406715	1.683967(-2)	1% at 35 km, $\chi = 85^\circ$
5	-3.281301(+2)	4.307004(+1)	-1.870019	2.674331(-2)		8% at 55 km, $\chi = 85^\circ$
6	-2.139117(+2)	2.612729(+1)	-1.036749	1.317695(-2)		9% at 70 km, $\chi = 85^\circ$
7	-8.334575(+1)	7.944254	-1.898894(-1)			15% at 75 km, $\chi = 85^\circ$
8	-1.213108(+3)	2.277459(+2)	-1.612207(+1)	5.101389(-1)	-6.090518(-3)	9% at 85 km, $\chi = 85^\circ$
9	-1.086239(+3)	1.981847(+2)	-1.359057(+1)	4.155845(-1)	-4.788462(-3)	14% at 65 km, $\chi = 85^\circ$
10	-3.701955(+1)	3.623290	-8.929223(-2)			25% at 40 km, $\chi = 85^\circ$
11	-2.431640(+3)	4.729722(+2)	-3.452121(+1)	1.120677	-1.365618(-2)	22% at 35 km, $\chi = 85^\circ$
12	-2.711900(+3)	5.369941(+2)	-3.988965(+1)	1.317533	-1.632895(-2)	19% at 40 km, $\chi = 85^\circ$
13	-1.986572(+3)	4.058984(+2)	-3.112428(+1)	1.061508	-1.358757(-2)	9% at 100 km, $\chi = 85^\circ$
14	-1.943757(+3)	3.918616(+2)	-2.966512(+1)	9.995864(-1)	-1.265243(-2)	13% at 50 km, $\chi = 85^\circ$
15	-7.008892(+2)	1.334594(+2)	-9.549089	3.048766(-1)	-3.675314(-3)	12% at 100 km, $\chi = 85^\circ$
16	-2.451485(+3)	5.174617(+2)	-4.096948(+1)	1.441835	-1.903091(-2)	20% at 60 km, $\chi = 85^\circ$
17	-2.507818(+3)	5.435242(+2)	-4.434785(+1)	1.613607	-2.208047(-2)	12% at 75 km, $\chi = 85^\circ$

* $\log_{10}c_i(z) = \sum_j b_{ij}[\log_{10}N(z)]^{j-1}$; $\sigma_i^e(z, \chi)/\sigma_i^e(z, \chi = 0^\circ) = (\sec\chi)^{-c_i(z)}$, where $N(z)$ is zenith column of oxygen in units of molecules cm^{-2} .

† Read 3.033416(+3) as $3.033416 \times 10^{+3}$.

$$\sigma_i^e(z, \chi)/\sigma_i^e(z, 0) = (\sec\chi)^{-c_i(z)} \quad (4)$$

and the coefficients $c_i(z)$ can be well fit by a polynomial expression

$$\log_{10}c_i(z) = \sum_j b_{ij}[\log_{10}N(z)]^{j-1}, \quad (5)$$

where $N(z)$ is the zenith O₂ column above altitude z (in units of molecules cm^{-2}). The variation of $\sigma_i^e(z, \chi)$ with χ is due to optical depth effects arising from the increasing O₂ column along the ray path with increasing zenith angle. The values of $c_i(z)$ and b_{ij} were determined by least-squares fits. The coefficients b_{ij} are presented in Table 3. The large maximum errors reported all occur when $T_i^e(z, \chi)$ is negligible, the average errors of the least-squares fit being significantly less (for example, in the case of I_{10} for which the maximum error is 25%, the error averaged over all altitudes for $\chi = 85^\circ$ is 4%).

Using the coefficients a_{ij} and b_{ij} , calculated effective cross sections $\sigma_i^e(z, \chi)$ are determined from (3)–(5) and can be used to compute the transmission $T_i^e(z, \chi)$ and O₂ photodissociation (with unit flux) $J_i^e(z, \chi)$, i.e.,

$$T_i^e(z, \chi) = \exp\left[-\int_z^\infty \sigma_i^e(z', \chi)n(z') \sec\chi dz'\right], \quad (6)$$

$$J_i^e(z, \chi) = \sigma_i^e(z, \chi)T_i^e(z, \chi)\Delta_i, \quad (7)$$

where $n(z')$ is the O₂ concentration at altitude z' . In Fig. 2, the relative errors in the computation of $T_i^e(z, \chi)$ are presented for each interval I_i for $\chi = 0, 30, 60$ and 85° . These errors result from errors in fitting the $\sigma_i^e(z, \chi)$ with simple polynomial functions. Also shown are the values for transmission at 50 and

80 km. Above the stratopause where O₂ photodissociation is dominated by the Schumann-Runge bands (Frederick and Hudson, 1980b), the errors are generally less than 20%. When the transmission becomes very small (less than a few percent), larger errors may occur, but this generally occurs in bands which have the lowest solar flux to start with. Errors in calculating $J_i^e(z, \chi)$ are very similar to what is shown in Fig. 2 for $T_i^e(z, \chi)$.

It is interesting to consider what systematic errors result from the assumption of the constancy of transmission and photodissociation values among different ray paths with equal O₂ columns. Since the high spectral resolution calculations for T_i and J_i were run for a relatively coarse altitude grid, there are only a few sets of ray paths with different zenith angles but the same O₂ column. Variances in the transmission values (from these detailed calculations) for ray paths with $\chi = 60$ or 85° relative to $\chi = 0^\circ$ values with the same O₂ column are displayed in Fig. 2. We find that, when the transmission is still relatively large ($\sim 10\%$), the "equivalent O₂ column" assumption may result in errors $\geq 20\%$ for some intervals. These errors are larger than the errors resulting from the approach of this paper.

The results of a number of recent analyses of observational data have bearing on the question of how well the opacity calculation technique proposed in this paper reproduces the real atmospheric transmission. Frederick *et al.* (1981) compare the results of detailed opacity calculations with data obtained from the first Solar Absorption Balloon Experiment (SABE-1) for the spectral range 184–202 nm. Above 194 nm, the agreement is at the 10% level, between 189 and 194 nm at the 20% level, and below 189 nm the

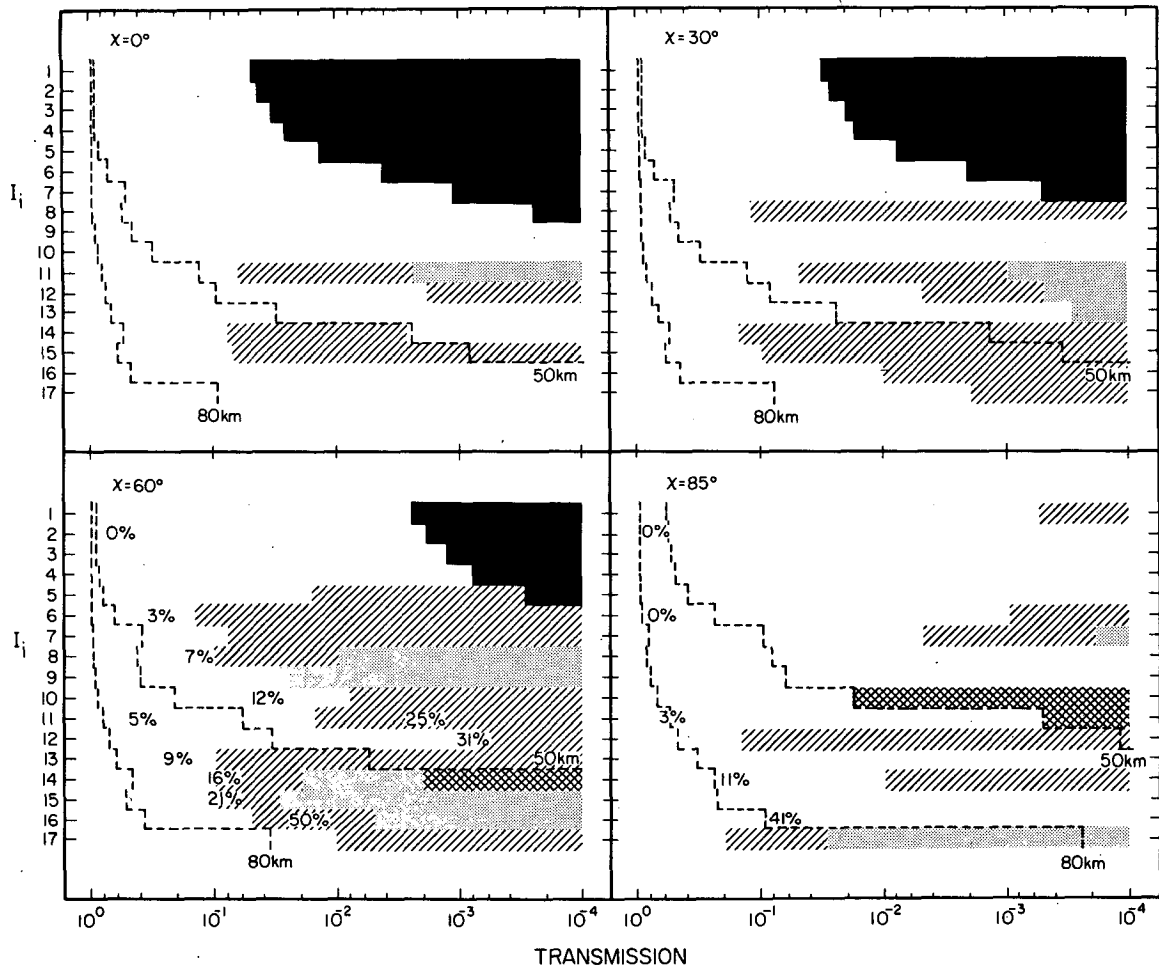


FIG. 2. Errors in calculated O_2 transmission values [0–10% (white area), 10–20% (diagonal shading), 20–30% (dots) and >30% (cross-hatched area)] for each interval I_i at solar zenith angles $\chi = 0, 30, 60$ and 85° . Also indicated are the values of $T_i(z, \chi)$ at 50 and 80 km (dashed lines). The current calculations do not extend below 20 km (indicated by the blacked-out area). The percentages shown are the variances between transmission values obtained from detailed calculations and values derived from the “equivalent O_2 column” assumption.

differences are as large as 40%. All the differences between the observational and theoretical results could well be due to uncertainties in the primary O_2

spectroscopic data that are the input to the detailed calculations. The spectral range 184–202 nm is covered by our intervals I_3 through I_{12} . At the illumi-

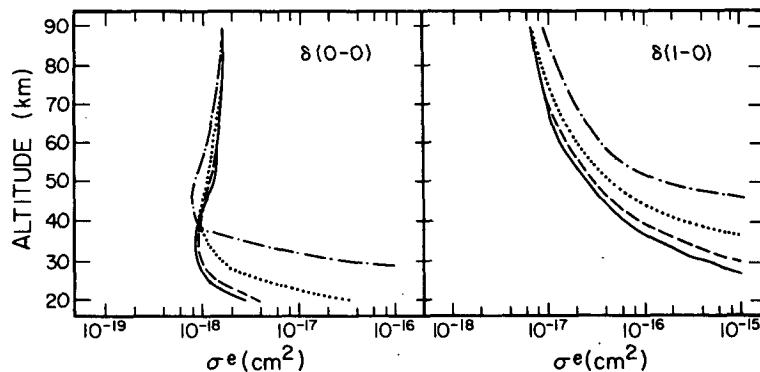


FIG. 3. Nitric oxide effective cross sections σ^e for the $\delta(0-0)$ and $\delta(1-0)$ bands for solar zenith angle $\chi = 0, 30, 60$ and 85° (same convention as in Fig. 1.)

nation conditions of SABE-1 (40 km altitude, $\chi = 34-42^\circ$), the transmission values calculated by the approach of this paper agree to better than 10% (see Fig. 2) with the same detailed calculations used in Frederick *et al.* (1981) and so are in just as good agreement with the SABE-1 results. A similar type of theoretical/observational comparison is done for the 200-210 nm range using the results of SABE-3. (Frederick and Mentall, 1982). At the short-wavelength end of this spectral range (covered to 206 nm by our intervals I_1 to I_3), the differences between theory and observations led Frederick and Mentall (1982) to suggest that the value of the O_2 Herzberg continuum cross section needed to be reduced by up to 15% below the lowest values in the literature (Shardanand and Prasad Rao, 1977). As the detailed calculations that were the precursor to the parameterization of this paper used Herzberg continuum cross sections larger than those of Shardanand and Prasad Rao (1977), the opacity values for I_1 through I_3 would be proportionally in disagreement with the SABE-3 data. However, when the correct values for the Herzberg continuum cross sections become more accurately known, the values for I_1 through I_3 can be simply adjusted since the predominant contribution to the total opacity at the wavelengths covered by I_1 through I_5 is the Herzberg continuum.

A slightly different approach to analyzing observed solar irradiances is taken by Herman and Mentall (1982) working with SABE-3 data between 190 and 230 nm. They invert the observed decrease in solar flux with decreasing altitude to obtain effective wavelength-dependent O_2 cross sections. Below 195 nm, their results are in good agreement with the effective cross sections calculated by us. Between 195 and 206 nm, their cross sections are systematically lower than our values and those of Shardanand and Prasad Rao (1977), leading them also to conclude that the Herzberg continuum cross sections need to be reduced. Froidevaux and Yung (1982) reach a similar conclusion after comparing observations with model calculations of species whose vertical distribution is sensitive to the intensity of the radiation near 200 nm. They find that model cross sections between 200 and 220 nm (200 through 206 nm being covered by I_1 through I_3) need to be reduced by 40% to obtain better observational/theoretical agreement. In light of these recent investigations, the reader can judge to what level of accuracy the results of the parameterizations of this paper reproduce true atmospheric transmission and can make simple adjustments when necessary.

3. Nitric oxide effective cross sections

Using the most up-to-date molecular constants, Frederick and Hudson (1979a) performed high spectral resolution calculations of the delta band predissociation of nitric oxide over the altitude range z

TABLE 4. Parametrization of NO effective photodissociation cross section σ^* .

Band	Polynomial coefficients										Maximum error of fit	
	a_1	a_2	a_3	a_4	a_5	a_6	a_7	a_8	a_9	a_{10}		
$\delta(0-0)$	-1.790868(+1)†	-1.924701(-1)	-7.217717(-2)	5.648282(-2)	4.569175(-2)	8.353572(-3)						2% at 40 km
$\delta(1-0)$	-1.654245(+1)	5.836899(-1)	3.449436(-1)	1.700653(-1)	-3.324717(-2)	-4.952424(-2)	1.579306(-2)	1.835462(-2)	3.368125(-3)			3% at 40 km

* $\log_{10}\sigma^*(z, \chi = 0^\circ) = \sum a_j [\log_{10} P(z)]^{j-1}$, where $P(z)$ is the pressure at altitude z and is in units of mb.

† Read -1.790868(+1) as -1.790868 $\times 10^{+1}$.

TABLE 5. Parameterization of zenith-angle dependence of NO effective photodissociation cross sections.*

Band	Polynomial coefficients					Maximum error of fit†
	b_1	b_2	b_3	b_4	b_5	
$\delta(0-0)$	7.836832(+3)‡	-1.549880(+3)	1.148342(+2)	-3.777754	4.655696(-2)	11% at 40 km, $\chi = 85^\circ$
$\delta(1-0)$	1.297581(+4)	-2.582981(+3)	1.927709(+2)	-6.393008	7.949835(-2)	36% at 55 km, $\chi = 85^\circ$

* $c(z) = \sum b_j [\log_{10} N(z)]^{j-1}$; $\sigma^e(z, \chi) / \sigma^e(z, \chi = 0^\circ) = (\sec \chi)^{c(z)}$, where $N(z)$ is zenith column of molecular oxygen in units of molecules cm^{-2} .

† Insignificant photodissociation rates ($< 10^{-10} \text{ s}^{-1}$) ignored.

‡ Read 7.836832(+3) as 7.836832×10^3 .

= 20–90 km for four solar zenith angles between 0 and 85° . The $\delta(0-0)$ band falls in the range of the Schumann-Runge bands I_8 and I_9 , and the $\delta(1-0)$ band in the range of I_{13} and I_{14} . Using their calcu-

lated photodissociation rates $J(z, \chi)$, the ozone zenith opacity they report for each band $\tau(\text{O}_3; z)$, and the solar flux F_i they used integrated for the relevant Schumann-Runge intervals I_i , effective cross sections were calculated,

$$\sigma^e(z, \chi) = \frac{J(z, \chi)}{[T_m^c(z, \chi)F_m + T_n^c(z, \chi)F_n] \exp[-\tau(\text{O}_3; z) \sec \chi]}, \quad (8)$$

where $m = 8$ and $n = 9$ for the $\delta(0-0)$ band and $m = 13$ and $n = 14$ for the $\delta(1-0)$ band.

The altitude variation of NO effective cross sections is shown in Fig. 3. At 90 km, the value of σ^e is close to the average absorption cross section for the particular NO δ band. The variation of σ^e with altitude cannot be readily interpreted, but in the case of each band, can be related to the local pressure; the zenith effective cross sections can be well fit by a simple polynomial expression

$$\log_{10} \sigma^e(z, \chi = 0^\circ) = \sum a_j [\log_{10} P(z)]^{j-1}. \quad (9)$$

Also, as is true for the O_2 effective cross sections, the zenith angle dependence of σ^e can be simply reproduced by

$$\sigma^e(z, \chi) / \sigma^e(z, 0) = (\sec \chi)^{c(z)} \quad (10)$$

and the zenith angle correction factors $c(z)$ can be parameterized as

$$c(z) = \sum b_j [\log_{10} N(z)]^{j-1}. \quad (11)$$

For each band, the coefficients a_j and b_j are determined by least-squares fits and are reported in Tables

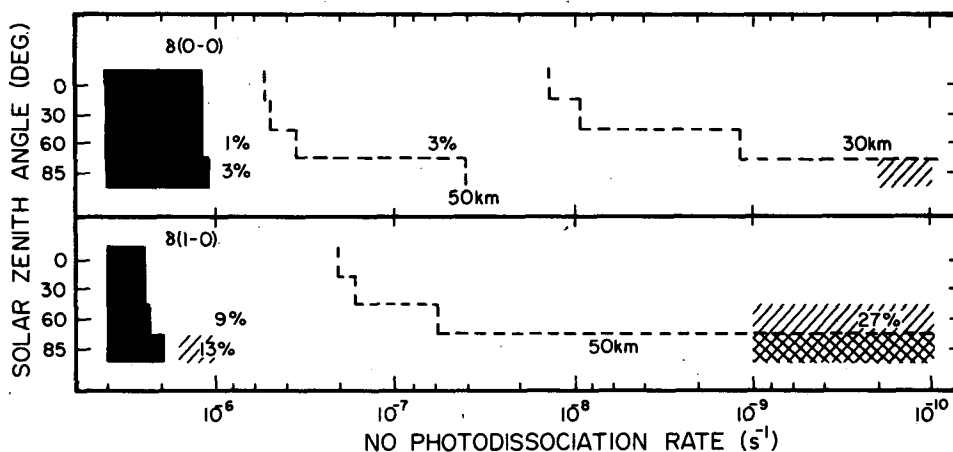


FIG. 4. Errors in calculated NO photodissociation rates—0–10% (white area), 10–20% (diagonal shading), 20–30% (dots) and >30% (cross-hatched area)—for the $\delta(0-0)$ and $\delta(1-0)$ bands at solar zenith angles $\chi = 0, 30, 60$ and 85° . Also indicated are the values of $J^e(z, \chi)$ at 30 and 50 km (dashed lines). The current calculations do not extend above 90 km (indicated by the blacked-out area). The percentages shown are the variances between transmission values obtained from detailed calculations and values derived from the “equivalent O_2 column” assumption.

4 and 5, respectively. The maximum errors for fitting σ_e (Table 4) are very small and are very similar to the mean error. The maximum errors reported in Table 5 are much larger than the average error; for example, in the case of the $\delta(1-0)$ band, the maximum error is 36% but the error averaged over all altitudes for which $\chi = 85^\circ$ and the photodissociation rate is $\geq 10^{-10} \text{ s}^{-1}$ is 12%. The error in approximating the zenith angle variation of σ_e can become large ($>30\%$) when $J(z, \chi)$ is very small ($\leq 10^{-9} \text{ s}^{-1}$) and unimportant for NO chemistry.

Since the calculated O_2 transmission values were used to compute σ_e for NO, the NO photodissociation rates $J^c(z, \chi)$ recomputed using T_i^c and σ_e (calculated) for NO [determined from (9)–(11) using a_j and b_j] are very close to the result of the high spectral resolution calculation. The errors in $J^c(z, \chi)$ relative to $J(z, \chi)$ are shown in Fig. 4 for both δ bands with $\chi = 0, 30, 60$ and 85° . Also displayed is the photodissociation rate for each band at 30 and 50 km. In the stratosphere and mesosphere, the errors in calculating J^c are very small, except for the $\delta(1-0)$ band at $\chi = 85^\circ$ at a point where its contribution to the total photodissociation rate is negligible.

As before, it is interesting to consider the systematic errors that would result from assuming equal photodissociation rates for ray paths with the same O_2 column. Using the results of high spectral resolution calculations (Frederick and Hudson, 1979a) for the few available pairs of ray paths with the same O_2 column, variances due to the "equivalent O_2 column" assumption were obtained and presented in Fig. 4. The comparison of results for ray paths with equivalent O_2 columns is complicated by the fact that the ozone mixing ratio is not constant above the tropopause, so there may be different amounts of ozone opacity in equivalent O_2 columns. When the detailed calculations are corrected for such differences, the variances obtained for points below 50 km are even larger than what is shown in Fig. 4. The systematic errors due to the equivalent O_2 column assumption are equal to or greater than the random errors arising from the approach of this paper. Moreover, the former errors may become appreciable at altitudes where NO photodissociation is significant.

4. Conclusion

The depth of the atmosphere to which solar radiation in the 175–200 nm spectral region penetrates is a sensitive function of the rotational line widths in the Schumann-Runge bands. The oscillator strength for each band measures the cross section integrated over the band while the line width determines how the absorption is distributed in wavenumber. The line widths of Frederick and Hudson

(1979b) tend to be less than those of previous studies and reasons for accepting the smaller values appear in the references given previously. Small line widths imply that the cross section tends to be concentrated in sharp peaks with less absorption occurring in regions far removed from line centers. The net effect is to allow more solar radiation to penetrate to lower altitudes in the atmosphere. Hence, smaller line widths imply that the 175–200 nm solar irradiance plays a greater role at lower altitudes than previously believed.

Photochemical modeling of the terrestrial atmosphere is facilitated by simple, but accurate, representations of high spectral resolution computations of opacity and dissociation in the Schumann-Runge band region. The approach taken in this paper leaves the choice of solar flux to the modeler. The coefficients reported can be easily recalculated if there are significant improvements in the more detailed Schumann-Runge band calculations.

Acknowledgments. We thank Y. L. Yung and L. Froidevaux for their helpful comments. This research was supported by JPL 49-649-20320-0-3270 to the California Institute of Technology. Contribution number 3621 of the Division of Geological and Planetary Sciences, California Institute of Technology.

REFERENCES

- Anderson, J. G., 1971: Rocket-borne ultraviolet spectrometer measurement of OH resonance fluorescence with a diffusive transport model for mesospheric photochemistry. *J. Geophys. Res.*, **76**, 4634–4652.
- Blake, A. J., 1979: An atmospheric absorption model for the Schumann-Runge bands of oxygen. *J. Geophys. Res.*, **84**, 3272–3282.
- Frederick, J. E., and R. D. Hudson, 1979a: Predissociation of nitric oxide in the mesosphere and stratosphere. *J. Atmos. Sci.*, **36**, 737–745.
- , 1979b: Predissociation line widths and oscillator strengths for the 2–0 to 13–0 Schumann-Runge bands of O_2 . *J. Mol. Spectrosc.*, **74**, 247–258.
- , 1980a: Atmospheric opacity in the Schumann-Runge bands and the aeronomical dissociation of water vapor. *J. Atmos. Sci.*, **37**, 1088–1098.
- , 1980b: Dissociation of molecular oxygen in the Schumann-Runge bands. *J. Atmos. Sci.*, **37**, 1099–1106.
- , R. D. Hudson and J. E. Mentall, 1981: Stratospheric observations of the attenuated solar irradiance in the Schumann-Runge band absorption region of molecular oxygen. *J. Geophys. Res.*, **86**, 9885–9890.
- , and J. E. Mentall, 1982: Solar irradiance in the stratosphere: implications for the Herzberg continuum absorption of O_2 . *Geophys. Res. Lett.*, **9**, 461–464.
- Froidevaux, L., and Y. L. Yung, 1982: Radiation and chemistry in the stratosphere: sensitivity to O_2 absorption cross sections in the Herzberg continuum. Submitted to *Geophys. Res. Lett.*
- Herman, J. R., and J. E. Mentall, 1982: O_2 absorption cross sections (190–225 nm) from stratospheric solar flux measurements. *J. Geophys. Res.* (in press).
- Hudson, R. D., V. L. Carter and E. L. Breig, 1969: Predissociation

- in the Schumann-Runge band system of O_2 : laboratory measurements and atmospheric effects. *J. Geophys. Res.*, **74**, 4079-4086.
- Kockarts, G., 1971: Penetration of solar radiation in the Schumann-Runge bands of molecular oxygen. *Mesospheric Models and Related Experiments*, G. Fiocco, Ed., D. Reidel, 160-176.
- , 1976: Absorption and photodissociation in the Schumann-Runge bands of molecular oxygen in the terrestrial atmosphere. *Planet. Space Sci.*, **24**, 589-604.
- Logan, J. A., M. J. Prather, S. C. Wofsy and M. B. McElroy, 1978: Atmospheric chemistry: response to human influence. *Phil. Trans. Roy. Soc. London A290*, 187-234.
- Nicolet, M., 1979: Photodissociation of nitric oxide in the mesosphere and stratosphere: simplified numerical relations for atmospheric model calculations. *Geophys. Res. Lett.*, **6**, 866-868.
- , and S. Cieslik, 1980: The photodissociation of nitric oxide in the mesosphere and stratosphere. *Planet. Space Sci.*, **28**, 105-115.
- , and W. Peetermans, 1980: Atmospheric absorption in the O_2 Schumann-Runge band spectral range and photodissociation rates in the stratosphere and mesosphere. *Planet. Space Sci.*, **28**, 85-103.
- Park, J. H., 1974: The equivalent mean absorption cross sections for the O_2 Schumann-Runge bands: application to the H_2O and NO photodissociation rates. *J. Atmos. Sci.*, **31**, 1893-1897.
- Shardanand, and A. D. Prasad Rao, 1977: Collision-induced absorption of O_2 in the Herzberg continuum. *J. Quant. Spectrosc. Radiat. Transfer*, **7**, 433-439.
- U.S. Standard Atmosphere, 1976*: U.S. Government Printing Office, Washington, DC.